Applied Energy 198 (2017) 145–159

Contents lists available at ScienceDirect

Applied Energy

journal homepage: www.elsevier.com/locate/apenergy

A stochastic optimization approach for the design of organic fluid mixtures for low-temperature heat recovery

M. Magdalena Santos-Rodriguez [a,c], Antonio Flores-Tlacuahuac [b], Victor M. Zavala [c,*]

[a] Energy Department, Universidad Autonoma Metropolitana-Azcapotzalco, Mexico City, Mexico
[b] Escuela de Ingenieria y Ciencias, Tecnologico de Monterrey, Campus Monterrey, Ave. Eugenio Garza Sada 2501, Monterrey, N.L. 64849, Mexico
[c] Department of Chemical and Biological Engineering, University of Wisconsin-Madison, Madison, WI, USA

HIGHLIGHTS

- A stochastic optimization approach is proposed to design organic heat transfer fluids.
- Risk metrics are used to design fluids that withstand strong variability in system conditions.
- Non-intuitive mixture compositions are identified.

ARTICLE INFO

Article history:
Received 8 November 2016
Received in revised form 7 April 2017
Accepted 15 April 2017

Keywords:
Design
Organic mixtures
Rankine cycle
Low-temperature
Uncertainty

ABSTRACT

Over 50% of the heat generated in industry is in the form of low-grade heat (with operating temperatures below 370 °C). Recovering heat from these sources with standard Rankine cycles (using water as working fluid) is inefficient and expensive. Organic working fluids have become an attractive alternative to mitigate these inefficiencies. In this work, we address the problem of designing flexible multi-component organic fluids capable of withstanding variability in heat source temperatures and efficiencies of individual cycle equipment units. The design problem is cast as a nonlinear stochastic optimization problem and we incorporate risk metrics to handle extreme variability. We show that a stochastic optimization framework allows us to systematically trade-off performance of the working fluid under a variety of scenarios (e.g., inlet source temperatures and equipment efficiencies). With this, it is possible to design working fluids that remain robust in a wide range of operational conditions. We also find that significant flexibility of the working fluid can be obtained by using optimal concentrations as opposed to using single component mixtures. We also find that state-of-the-art nonlinear optimization solvers can handle highly complex stochastic optimization problems that incorporate detailed physical representations of the system.

1. Introduction

Low-grade heat is a low-temperature (below 370 °C) heat source that is deemed too inefficient/expensive to recover [1,2]. Over 50% of the total heat generated in industry is in the form of low-grade heat [3]. In the cement industry, for instance, 40% of the heat available for recovery is lost to the environment via flue gases (at temperatures in the range 215–315 °C) [4]. According to the US Department of Energy, 33% of the energy used in the manufacturing sector is waste heat and approximately 60% of this waste heat is at temperatures below 230° [2]. Power generation is an important source of waste heat, which include: liquid streams (50–300 °C), stack losses (150–180 °C), steam losses (100–250 °C), and processing gases and vapors (80–300 °C). Low-grade heat is also found in emerging sustainable power generation technologies that include concentrated solar (below 300 °C), biomass-based (150–320 °C), and geothermal power generation (60–200 °C) [5,1,6]:

The conventional Rankine cycle (steam power cycle) has long been the workhorse in power generation. These systems use water as working fluid which makes the recovering of low-grade waste heat inefficient and expensive [7]. This is because water, while inexpensive and scalable, has limited thermodynamic flexibility. The Organic Rankine Cycle (ORC) provides a more attractive avenue to recover low-grade heat. In this cycle, an organic heat transfer fluid with low-boiling point and high vaporization enthalpy is used to drive the cycle [8,7,9–12]. An organic multiple component

* Corresponding author at: Department of Chemical and Biological Engineering, University of Wisconsin-Madison, 1415 Engineering Drive, Madison, WI, 53706, USA.
E-mail address: victor.zavala@wisc.edu (V.M. Zavala).

http://dx.doi.org/10.1016/j.apenergy.2017.04.047
0306-2619/

mixture can also be used to target thermodynamic properties that maximize cycle efficiency and flexibility [13]. ORCs are currently being used in diverse sustainable power generation systems [14,15], as shown in Fig. 1.

Recent reports have shown that, compared to the use of single organic fluids, multicomponent mixtures can significantly enhance the power efficiency of low-temperature heat recovery Rankine cycles [16,17]. In this context, an important related problem consists in determining the optimal blending of organic fluids. Diverse studies exist in the literature on the evaluation, selection, and design of multicomponent organic fluid mixtures and on the optimization of ORC operations. In particular, Papadopoulos and co-workers presented a computer-aided molecular design method for the synthesis and selection of binary working fluid mixtures used in ORCs [18]. Yin and co-workers investigated mixtures of SF_6-CO_2 as working fluids for geothermal power plants [19]. Shu and co-workers studied mixtures based on blending of hydrocarbon with refrigerant retardants used in ORC [20]. Andreasen and co-workers presented a methodology for ORC optimization based on multicomponent mixtures [21]. The use of zeotropic mixtures in ORC is explored in [22–29]. More recently, Molina-Thierry and co-workers used a simultaneous optimal design approach for organic mixtures and ORC operation [9]. Liu and co-workers optimized and analyzed a geothermal organic Rankine using mixtures of R600a and R601a [30]. Fen and co-workers used multi-objective optimization for performance of low-grade ORC using R245fa and pentane [31,32]. Habka and co-workers evaluated the performance of organic mixtures in ORC using geothermal water as heat source [33]. Sadeghi and co-workers presented a thermodynamic analysis and used multi-objective optimization techniques to design zeotropic mixtures [28]. Papadopoulos et al. presented a sensitivity analysis on the effect of different system and fluid parameters on the performance of ORCs [18,34,35]. Recently, Frutiger et al. [36] used a Monte Carlo simulation procedure to evaluate the performance of fluid mixtures in the face of system uncertainties. High-throughput screening of working fluids using detailed thermodynamic and process simulations is reported in [37]. Additional applications of ORCs in industry have also been addressed [38–40].

In this work, we address the problem of designing multicomponent organic fluid mixtures capable of achieving optimal performance in the face of uncertainty in heat source temperatures and efficiencies of individual components of the ORC. The design problem is cast as a stochastic optimization problem and we use risk metrics to trade-off flexibility and average performance. We show that the methodology can identify new and non-intuitive heat transfer fluid mixtures that withstand extreme variability in system conditions while maintaining close-to-optimal performance. To the best of our knowledge, our work is the first to propose the combine advanced stochastic optimization techniques and first-principles modeling to design multi-component heat transfer fluids. We highlight that the stochastic optimization approach finds a single optimal design for a fluid mixture that behaves optimally under a range of uncertainties. Monte Carlo and sensitivity techniques reported in the literature, on the other hand, evaluate performance of different fluids under multiple scenarios but cannot systematically identify a single fluid that works best in all scenarios. We also highlight that our proposed approach simultaneously identifies an optimal composition for the fluid mixture and optimal operating conditions for the ORC. This simultaneous approach is necessary to capture dependencies between the physical properties of the heat transfer fluid and the operating conditions of the system.

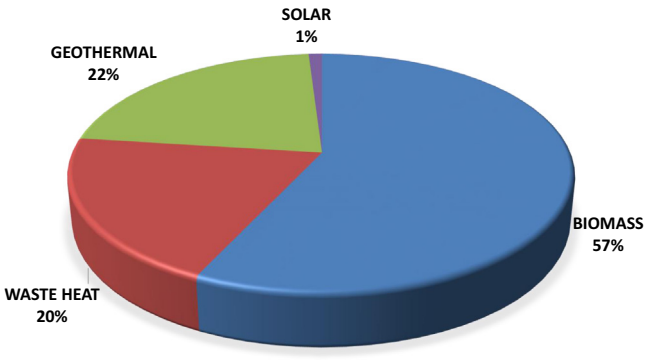

Fig. 1. Current applications of ORC in industry [1].

The paper is structured as follows. In Section 2 we describe ORCs. In Section A we present an optimization formulation that seeks to maximize the overall cycle efficiency by determining an optimal composition of the mixture and operating conditions for the ORC units while satisfying thermodynamic equilibrium conditions, conservation equations, and constraints. In Section 3 we discuss how to extend this formulation to account for uncertainty (variability) in operational factors affecting the performance of the cycle. Case studies are presented in Section 4.

2. Organic Rankine cycles

An ORC converts low-grade heat to electricity by using an organic working fluid instead of water. Organic working fluids have lower boiling points than water and thus can be used to recover heat at lower temperatures [10,7]. The ORC (see Fig. 2) uses the same equipment as a conventional Rankine cycle. It consists of an evaporator (heating area), a turbine, a condenser (cooling area), and a pump [5,9]. As shown in Fig. 2, the ORC is composed of the following steps:

1. Constant pressure heating of the working fluid to a superheated vapor state.
2. Expansion of the vapor to a low pressure level.
3. Constant pressure cooling of gas until condensation conditions are reached.
4. Compression at high pressure level.

The cycle performance strongly depends on the thermodynamic properties of the working fluid [41,35]. When a multicomponent mixture is used as working fluid, operational efficiency can be increased [42,9,18,34]. In particular, by altering its composition, we can implicitly manipulate: (i) Temperature gradients at phase equilibria, (ii) pressure ratios, and (iii) the superheating degree. Thermodynamic cycle analysis shows that, for a pure component under a constant-pressure phase change, the temperature remains constant (see Fig. 3). In the two-phase region, the process starts and ends at the saturation temperature ($T_{Be} = T_{De}$). For a multicomponent mixture, on the other hand, the phase change occurs at a range of temperatures and compositions (i.e., $T_{Be} \neq T_{De}$) [9]. This nonisothermal phase change of the mixture allows for a much better match between the temperature profiles of the working fluid and of the heat source [43]. In Fig. 4 we illustrate this behavior. In particular, we show five points: three internal points ($N_\Psi = 3$) that represent the vaporization fraction Ψ_f and the bubble and dew points; P_{Low} and P_{High} are pressure levels as well as the isentropic points subcoolS (subS) and overheatS(overS) that correspond to compression and expansion points, respectively.

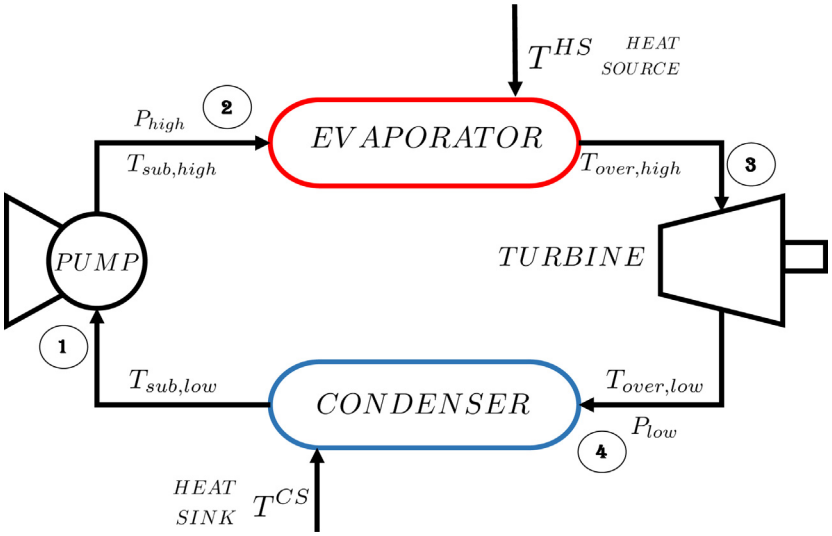

Fig. 2. Schematic of a ORC.

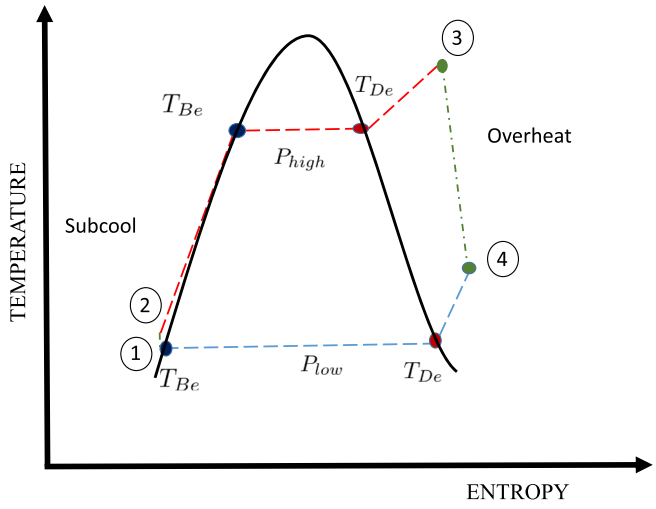

Fig. 3. T-s diagram of pure component.

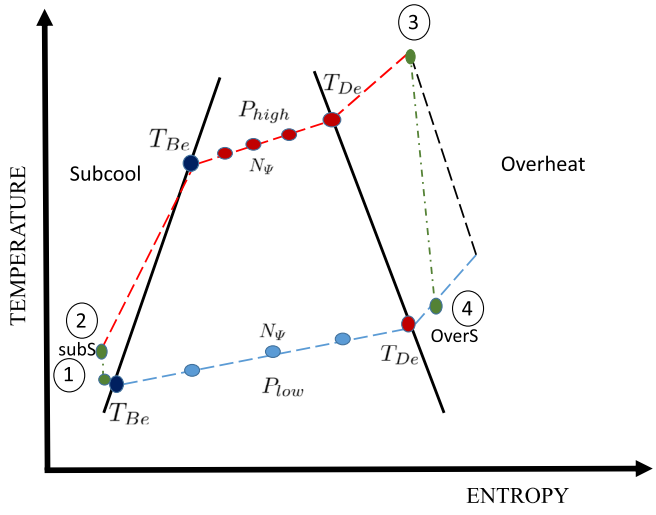

Fig. 4. T-s diagram for mixture.

3. Stochastic optimization formulation

The optimization problem under study seeks to determine an optimal composition of a mixture of given components in order to maximize the overall cycle efficiency of the ORC [43]. The maximization of the overall efficiency seeks to generate the best net output to input ratio of energy [9]. A detailed formulation of this deterministic optimization problem is presented in Appendix A. All variables are defined in Appendix B. This deterministic optimization formulation can be written in compact form as:

$$\begin{aligned} \min_{x,y} \quad & f(x,y,\xi) \\ \text{s.t.} \quad & g(x,y,\xi) \geqslant 0, \end{aligned} \tag{3.1}$$

where x are design variables (mixture compositions), y operational variables (pressures, temperatures, enthalpies, and so on), and ξ are parameters (heat source temperatures, equipment efficiencies, physical parameters). The cost function $f(\cdot)$ is the negative overall cycle efficiency (we maximize efficiency). We note that the above optimization formulation assumes a given value for the parameters ξ but does not factor in uncertainty on such parameters. We now proceed to describe stochastic formulations that are capable of doing this.

We assume that the parameters are realizations of a discrete random variable Ξ (denoted as $\xi_1, \ldots, \xi_n$) and with corresponding probabilities $p_{\xi_1}, \ldots, p_{\xi_n}$. The realizations are encapsulated in an scenario set $\Omega := \{\xi_1, \ldots, \xi_n\}$. We use these definitions to formulate the following stochastic optimization problem:

$$\begin{aligned} \min_{x,y(\Xi)} \quad & \mathbb{E}[\varphi(x,y(\Xi),\Xi)] \\ \text{s.t.} \quad & g(x,y(\xi),\xi) \geqslant 0, \quad \xi \in \Omega, \end{aligned} \tag{3.2}$$

where $\mathbb{E}[\Xi]$ is the expectation of an arbitrary random variable Ξ and is given by $\sum_{\xi \in \Omega} p_\xi \xi$. The function $\varphi(\cdot)$ is a general function that is used to represent different statistics of the random cost $f(x,y(\Xi),\Xi)$ (e.g., mean, variance, worst-case, conditional value at risk). We consider these cases individually in the next subsections.

In the stochastic optimization formulation, the goal is to find a design variable x and corresponding recourse variables $y(\Xi)$ such that a given statistic is minimized. In other words, a stochastic program gives a single decision x that works best in some statistical sense (e.g., on average or in the worst-case) over a set of scenarios

Ω. In our case, x is the composition of the working fluid that we seek to design.

It is also often of interest to solve the so-called *perfect information* problem in which we assume that we can identify an optimal design $x(\xi)$ for each scenario $\xi \in \Omega$. These *ideal* designs are obtained by solving the problem:

$$\min_{x(\Xi),y(\Xi)} \quad \mathbb{E}[\varphi(x(\Xi),y(\Xi),\Xi)] \tag{3.3a}$$

$$\text{s.t.} \quad g(x(\xi),y(\xi),\xi) \geqslant 0, \quad \xi \in \Omega, \tag{3.3b}$$

Clearly, the designs $x(\Xi)$ are unattainable (in our context this would imply that we can change our working fluid in each scenario $\xi \in \Omega$). The perfect information designs, however, can be used as a baseline to compare optimal designs obtained from (3.2).

In summary, the optimization strategy employed in this work involves the following tasks.

- *Selection of the uncertain parameters*. First, we select the uncertain parameters in our optimization model that have most influence on the performance on the ORC.
- *Perfect Information design*. We obtain an optimal design for each scenario under the perfect information assumption.
- *Stochastic design*. We find a single optimal design that performs best (in some statistical sense) in all scenarios.

3.1. Expected value

When $\varphi(\cdot) = f(\cdot)$ we have that the objective function in (3.2) is simply:

$$\mathbb{E}[\varphi(x,y(\Xi),\Xi)] = \sum_{\xi\in\Omega} p_\xi f(x,y(\xi),\xi). \tag{3.4}$$

Here, the goal is to find a design that works best on average. This design, however, does not control the system performance in tail (extreme) scenarios.

3.2. Risk measures

We use risk metrics to shape the behavior of the ORC design in extreme scenarios [44,45]. We consider the variance and the conditional value at risk (CVaR).

3.2.1. Variance

The variance is a measure of dispersion of the cost $f(x,y(\Xi),\Xi)$. By using

$$\varphi(x,y(\Xi),\Xi) \;:=\; (f(x,y(\Xi),\Xi) - \mathbb{E}[f(x,y(\Xi),\Xi)])^2 \tag{3.5}$$

in (3.2), we note that the objective function becomes:

$$\mathbb{V}[f(x,y(\Xi),\Xi)] = \mathbb{E}\Big[(f(x,y(\Xi),\Xi) - \mathbb{E}[f(x,y(\Xi),\Xi)])^2\Big]. \tag{3.6}$$

The variance allows the decision-maker to narrow down the tails of the cost distribution associated to extreme scenarios. With this, the goal is to find a design that has reduced variability in performance. The variance minimization approach can be seen as way to improve flexibility (by ensuring that the system behaves as close as possible to the mean for all scenarios). Since the mean and the variance are often conflicting, they are typically handled simultaneously by minimizing a weighted mean-variance objective. This corresponds to using

$$\varphi(x,y(\Xi),\Xi) \;:=\; f(x,y(\Xi),\Xi) + \kappa(f(x,y(\Xi),\Xi) - \mathbb{E}[f(x,y(\Xi),\Xi)])^2 \tag{3.7}$$

in (3.2) and we note that the objective function simply becomes $\mathbb{E}[f(x,y(\Xi),\Xi)] + \kappa\mathbb{V}[f(x,y(\Xi),\Xi)]$. Here, $\kappa \geqslant 0$ is the trade-off weight.

The variance has been subjected to some criticism because it penalizes deviations around the mean symmetrically (i.e., on both sides of the mean) [44]. This is undesirable in applications like ORC design where we are only interested in penalizing deviations below the mean efficiency (i.e., we seek to keep the ones above the mean efficiency intact).

3.2.2. Conditional Value Risk (CVaR)

The value-at-risk (VaR) of the random variable Ξ is defined as the critical value t at which the probability of Ξ being below such critical value is greater than $1-\alpha$ (i.e., VaR is a quantile of Ξ). Mathematically, this is given by [46]:

$$\text{VaR}_{1-\alpha}(\Xi) \;:=\; \min\{t | P(\Xi \leqslant t) \geqslant 1-\alpha\} \tag{3.8}$$

VaR is rarely used as a risk metric because it is difficult to handle computationally. An alternative risk measure is the Conditional Value-at-Risk (CVaR) [47]. CVaR can be defined as the conditional expectation of Ξ in excess of VaR (e.g., average costs larger than VaR). Mathematically,

$$\text{CVaR}_{1-\alpha}(\Xi) \;:=\; \mathbb{E}[\Xi | \Xi \geqslant \text{VaR}_{1-\alpha}(\Xi)]. \tag{3.9}$$

Interestingly, CVaR can be computed as the solution of the optimization problem:

$$\text{CVaR}_{1-\alpha}(\Xi) = \inf_t \left\{ t + \frac{1}{\alpha}\mathbb{E}[\Xi - t]_+ \right\} \tag{3.10}$$

and it is easy to show that value of t that minimizes the right-hand side (denoted as t^*) is:

$$t^* = \text{VaR}_{1-\alpha}(\Xi). \tag{3.11}$$

We can formulate a stochastic optimization problem to minimize CVaR in the form (3.2) by defining:

$$\varphi(x,y(\Xi),\Xi) \;:=\; \inf_t \left\{ t + \frac{1}{\alpha}[f(x,y(\Xi),\Xi) - t]_+ \right\}. \tag{3.12}$$

It is well-known that the CVaR minimization problem can be reformulated as:

$$\begin{aligned} \min_{x,y(\Xi),t} \quad & \mathbb{E}\left[t + \frac{1}{\alpha}\varphi(\Xi) \right] \\ \text{s.t.} \quad & f(x,y(\xi),\xi) - t \leqslant \varphi(\xi), \quad \xi \in \Omega \\ & g(x(\xi),y(\xi),\xi) \geqslant 0, \quad \xi \in \Omega \\ & \varphi(\xi) \geqslant 0, \quad \xi \in \Omega. \end{aligned} \tag{3.13}$$

A key property of $\text{CVaR}_{1-\alpha}(\Xi)$ is that it converges to the expected value ($\mathbb{E}[\Xi]$) when $\alpha \to 1$ and to the worst-case value (denoted as $\text{ess sup}\,\Xi$) when $\alpha \to 0$. The convergence property to the worst-case can be established by noticing that CVaR can be written as:

$$\text{CVaR}_{1-\alpha}(\Xi) = \text{VaR}_{1-\alpha}(\Xi) + \alpha^{-1}\mathbb{E}[\Xi - \text{VaR}_{1-\alpha}(\Xi)]_+ \tag{3.14}$$

and by noticing that $\lim_{\alpha\to 0}\text{VaR}_{1-\alpha}(\Xi) = \text{ess sup}[\Xi]$ and thus $\lim_{\alpha\to 0}\mathbb{E}[\Xi - \text{VaR}_{1-\alpha}(\Xi)]_+ = 0$. Convergence to the expected value can be established by noticing that $\lim_{\alpha\to 1}\text{VaR}_{1-\alpha}(\Xi) = \text{ess inf}[\Xi]$ (the smallest value of Ξ) and thus $\lim_{\alpha\to 1}\mathbb{E}[\Xi - \text{VaR}_{1-\alpha}(\Xi)]_+ = \mathbb{E}[\Xi] - \text{ess inf}[\Xi]$.

Another key property that is often not highlighted in the literature is that CVaR is in fact a weighted sum of $\mathbb{E}[\Xi]$ and of an *asymmetric dispersion metric* of Ξ (that we denote as $\mathbb{D}_\kappa$). Mathematically, we have that CVaR satisfies:

$$\text{CVaR}_{1-\alpha}[\Xi] = \mathbb{E}[\Xi] + \mathbb{D}_\kappa[\Xi] \tag{3.15}$$

with

$$\mathbb{D}_\kappa[\Xi] \;:=\; \inf_t \mathbb{E}\{[t-\Xi]_+ + \kappa[\Xi - t]_+\}. \tag{3.16}$$

and $\kappa = \frac{\alpha}{1-\alpha}$. Here, again, the value of t that minimizes the right-hand side is simply $t^* = \text{VaR}_{1-\alpha}(\Xi)$. CVaR thus simultaneously minimizes the expected value and penalizes deviations above VaR by using a weight $\kappa \geqslant 1$ that becomes larger and larger as $\alpha \to 1$ (values below VaR are penalized by using a weight of one). This asymmetric penalization property provides a key benefit over the mean-variance formulation and highlights that CVaR naturally trades-off average and variability.

4. Case studies

We base our case study on the setting of Molina-Thierry and Flores-Tlacuahuac [9]. In that work, the authors studied the design of working fluids for ORCs using low-temperature sources and the system parameters shown in Table 1. Assumptions made for the cycle modeling are: The working fluid is a heat source in liquid state and the heat sink source is water liquid at 20 °C, while the composition of mixture is given in mole fraction. The basis used for computations is 1 mol. We highlight that all compositions reported in the tables are dimensionless and all the temperatures are in °C. All optimization models and data needed to reproduce the results can be found in http://zavalab.engr.wisc.edu/data.

It should be stressed that in Table 1 N_Ψ represents the internal points in the region of two phases (evaporator and condenser). Each internal point has a vaporization fraction named Ψ_f. We considered three internal points.

4.1. Performance of single and multi-component mixtures

We first solve a deterministic model to illustrate how the use of multi-component mixtures can improve ORC efficiency. We consider a heat source with a temperature of $T^{HS,IN} = 150$ °C. In Table 2 we compare the overall cycle efficiency η for three different configurations. In the first configuration we maximized the efficiency of the ORC using an organic mixture (*n*-butane and *n*-pentane), in the second configuration we maximized the efficiency of ORC using a pure component (*n*-pentane), and in the third configuration we calculated the efficiency for a conventional Rankine cycle that uses water as working fluid. As can be seen, the organic mixture achieves an efficiency of over 18% while the standard Rankine cycle can only achieve and efficiency of 2.6% (an improvement of a factor of three). We also note that the efficiency of the single component fluid is lower by only 1% but this can indeed translate in significant losses in large-scale generation systems.

4.2. Stochastic designs

We are interested in designing a working fluid capable of withstanding uncertainty (variability) in factors affecting the operation of the ORC. In particular, we consider variability in the temperature of the heat source (denoted as $T^{HS}(\Xi)$) and in the turbine efficiency (denoted as $\eta_T(\Xi)$). In a first case we only consider variability in $T^{HS}(\Xi)$ at keep $\eta_T(\Xi)$ fixed. In a second case we consider variability in $\eta_T(\Xi)$ and keep $T^{HS}(\Xi)$ fixed. In the third case we consider simultaneous variability in turbine efficiency and heat source temperature. These studies are designed so as to understand the factors that have the strongest effect on the operation and how those influence the optimal composition of the organic mixture. In our formulation, we treat the composition of four components as first-stage (design) variables while the rest of the operational variables are two-stage (recourse) variables. We consider an organic mixture containing four possible components: pentafluoropropane ($C_3H_3F_5$), dodecafluoropentane (C_5F_{12}), butane (C_4), and pentane (C_5).

Table 1
Parameters for case study.

Parameter	Value	Units
$T^{HS.IN}$	423.15(150)	K (°C)
$T^{CS.IN}$	293.15(20)	K (°C)
η_{SP}	0.9	–
η_{ST}	0.9	–
ΔT^{CS}	10	K (°C)
ΔT^{HS}	20	K (°C)
ΔP_{min}	1	bar
ΔT_{min}	5	K
R_g	8.314	kJ kmol^{-1} K^{-1}
N_Ψ	3	–

Table 2
Optimal performance of single and multi-component organic fluids.

$T^{HS,IN}$ (°C)	150		
	ORC		Standard RC
	Multi-comp	Single-comp	Single-comp
z_{C_4}	0.35	–	–
z_{C_5}	0.65	1.00	–
z_{H_2O}	–	–	1.00
η	18.2%	16.7%	2.6%
W_{net} (kJ kmol^{-1})	7112	6345	1168
q_{IN} (kJ kmol^{-1})	39,076	37,841	44,964
CPU time (s)	9.4	7.4	10.1
# variables	3283		

4.2.1. Case I. Uncertainty in heat source temperature

We consider a heat source temperature that varies in the range of 130—150 °C and we span this range using five scenarios. In this case, we use a fixed turbine efficiency of 90%. We first evaluate the impact of the heat source temperature on efficiency and on the optimal composition of the working fluid mixture. This is done by solving the perfect information problem (3.3). We note that this case is equivalent to performing sensitivity analysis and does not give an implementable organic working fluid design because the composition is allowed to be changed at each temperature. This solution, however, can be used to set an ideal reference of performance, as the organic fluid to be designed cannot exceed the efficiency of the perfect information designs. The results are presented in Table 3. We can observe that, in all cases, a multi-component mixture is needed to maximize efficiency. We also note that the composition changes drastically at different temperatures but the composition of *n*-pentane persists in all cases and dominates the mixture. Interestingly, at high temperatures, the optimal fraction of *n*-butane is large (16–35%) but decreases rapidly as the temperature of the source is decreasing. At medium temperatures, $C_3H_3F_5$ becomes a more efficient alternative while at low temperatures C_5F_{12} becomes more prominent. We also see that the optimal efficiency of the cycle decays from 18.3% to 16.2% as the temperature of the heat source is decreased. We can thus see that there is significant variability in the ORC designs.

We now solve the stochastic optimization problem (3.2) to find an optimal working fluid that maximizes the mean efficiency over the heat source temperature range. The results are presented in Table 4. We find that the optimal composition for the considered heat source range is a binary mixture composed of 79% *n*-pentane and 21% *n*-butane. We see that the average maximum cycle efficiency is 16.9% while the efficiencies for each scenario span the range 17.1–16.2%. We highlight that (as expected) these efficiencies are inferior to those of the perfect information cases (in which we assume that the composition can be adjusted in each scenario).

We explore the existing trade-offs of mean efficiency and performance at extreme temperatures. To do so, we consider a

Table 3
Perfect information design for Case I: variability in $T^{HS}(\Xi)$ and fixed $\eta_T(\Xi) = 90\%$.

	$T^{HS}(\Xi)$ in (°C)				
	130	135	140	145	150
$z_{C_3H_3F_5}$	0.194	0.280	0.298	0.028	–
$z_{C_5F_{12}}$	0.099	0.043	–	–	–
z_{C_4}	–	–	–	0.161	0.35
z_{C_5}	0.707	0.677	0.702	0.811	0.65
$\eta(\Xi)$	16.3%	16.9%	17.5%	17.9%	18.2%
$\mathbb{E}[\eta(\Xi)]$			17.4%		

Table 4
Stochastic design for Case I: variability in $T^{HS}(\Xi)$ and fixed $\eta_T(\Xi) = 90\%$.

	$T^{HS}(\Xi)$ in (°C)				
	130	135	140	145	150
$z_{C_3H_3F_5}$			–		
$z_{C_5F_{12}}$			–		
z_{C_4}			0.211		
z_{C_5}			0.789		
$\eta(\Xi)$	16.2%	16.8%	17.1%	17.1%	17.1%
$\mathbb{E}[\eta(\Xi)]$			16.9%		

stochastic optimization model that maximizes mean efficiency and minimizes variance (Table 5). We span the trade-off weights to compute different Pareto solutions. The results are illustrated in Fig. 5. As can be seen, as the mean efficiency increases, so does the variance and thus the performance degrades at the extremes of the heat source temperature range. We also note that the variance strongly penalizes deviations around the mean and we see that it degrades performance at high temperatures, which is undesired. Again, this is due to the symmetric penalization induced by the variance.

We now explore the optimal designs for CVaR as we span the range of $\alpha \in [0, 1]$ (Table 6). For $\alpha = 1/5$ we can observe that minimizing CVaR is improving the worst case efficiency of the expected value design from 16.2% to 16.5% and we see that the system has the same efficiency in all scenarios. We can thus see that the performance of this design is robust. We also note that this solution has essentially zero variance but, interestingly, this solution is not identified by the mean-variance approach. This again highlights that the variance is not a desirable dispersion metric.

4.2.2. Case II. Uncertainty in turbine efficiency

In our second case study we want to find an optimal mixture for the ORC that is robust to variability in turbine efficiency $\eta_T(\Xi)$. We span a turbine efficiency range of 90–70% with 5 scenarios. We highlight that we use this range to demonstrate our methodology, but we acknowledge that lower efficiencies can be observed in actual practice. In this case, we keep the heat source temperature at 150 °C. The perfect information designs for this case are shown

Table 5
Mean-variance designs for Case I: variability in $T^{HS}(\Xi)$ and at fixed $\eta_T(\Xi) = 90\%$.

	$T^{HS}(\Xi)$ in (°C)	130	135	140	145	150
1	$\eta(\Xi)$	16.0%	16.8%	16.8%	16.8%	16.8%
	$\mathbb{E}[\eta(\Xi)]$			16.6%		
	$\mathbb{V}(\eta(\Xi))$			271.6		
2	$\eta(\Xi)$	14.0%	14.0%	14.0%	14.0%	14.0%
	$\mathbb{E}[\eta(\Xi)]$			14.0%		
	$\mathbb{V}(\eta(\Xi))$			190.9		
3	$\eta(\Xi)$	11.3%	11.3%	11.3%	11.3%	11.3%
	$\mathbb{E}[\eta(\Xi)]$			11.3%		
	$\mathbb{V}(\eta(\Xi))$			124.5		
4	$\eta(\Xi)$	8.58%	8.58%	8.58%	8.58%	8.58%
	$\mathbb{E}[\eta(\Xi)]$			8.58%		
	$\mathbb{V}(\eta(\Xi))$			72.13		
5	$\eta(\Xi)$	5.89%	5.89%	5.89%	5.89%	5.89%
	$\mathbb{E}[\eta(\Xi)]$			5.89%		
	$\mathbb{V}(\eta(\Xi))$			34.0		
6	$\eta(\Xi)$	3.20%	3.20%	3.20%	3.21%	3.19%
	$\mathbb{E}[\eta(\Xi)]$			3.2%		
	$\mathbb{V}(\eta(\Xi))$			10.04		
7	$\eta(\Xi)$	0.49%	0.49%	0.49%	0.49%	0.59%
	$\mathbb{E}[\eta(\Xi)]$			0.51%		
	$\mathbb{V}(\eta(\Xi))$			0.257		

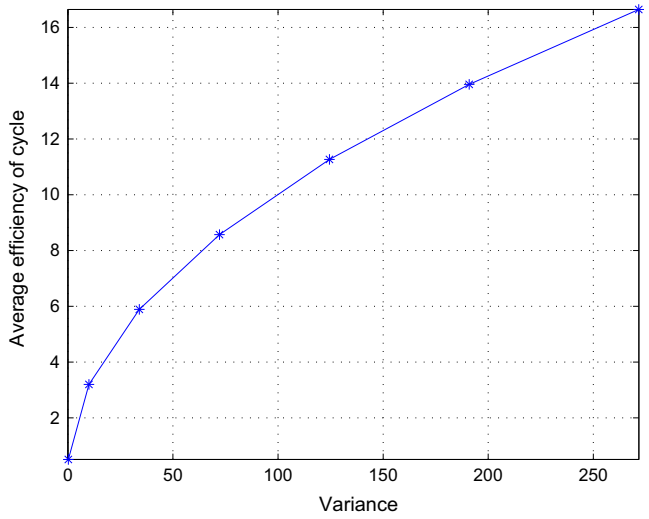

Fig. 5. Mean-variance trade-off curve for Case I.

in Table 7. We can see that the turbine efficiency has a stronger effect on overall cycle efficiency than the temperature of the heat source. The overall cycle efficiency changes from 18.4% to 14.2%. Interestingly, we note that, in this case, $C_3H_3F_5$ becomes a more prominent component in the mixture but pentane is still the dominant one.

In the case of the stochastic design shown in Table 8, we see that the optimal mixture is composed of nearly 96% C_5F_{12} and 4% *n*-butane. We can see this working fluid as one that achieves an optimal compromise among the scenarios. This highlights that certain component mixtures are more efficient than others at absorbing variability in system conditions. We also highlight that the compromise solution obtained with stochastic optimization achieves efficiencies in the range 14.5–11.1%, which are clearly lower than those of the perfect information solution. For the case of CVaR, we found in this case that all solutions are the same as we span $\alpha = [0, 1]$. This is shown in Table 9. This result implies that the system has limited flexibility to mitigate extreme events in component efficiencies.

4.2.3. Case III: Uncertainty in heat source temperature and turbine efficiency

In our last case we want to find an optimal mixture considering uncertainty in both the heat source temperature $T^{HS}(\Xi)$ and the turbine efficiency $\eta_T(\Xi)$. We create all possible permutations for the five scenarios in each case to create a set of 25 scenarios. As show in Table 10, the optimal mixture is composed of nearly 40% butane and 60% *n*-pentane. We note that the efficiency $\eta(\Xi)$ is in the range 18.2–12.2% and, as expected, the best efficiency obtained at 150 °C and a turbine efficiency of 90% while the worst efficiency is observed at a temperature of 130 °C and with an efficiency in the turbine of 70%. An interesting finding is that the optimal overall cycle efficiencies for scenarios with a turbine efficiency of 90% and that span the heat source temperature, are very close to the perfect information efficiencies shown in Table 3 and are much higher than the stochastic design efficiencies shown in Table 4. Similarly, the optimal efficiencies for scenarios with heat source temperature at 150 °C and that span the turbine efficiency, are very close to the perfect information efficiencies shown in Table 7 and are much higher than the stochastic design efficiencies of Table 8. From these results we can conclude that the stochastic designs of Tables 4 and 8 are local solutions and that the addition of more scenarios aids the optimizer to find high-quality solutions.

The results for CVaR designs are shown in Tables 11 and 12. As can be seen, as we decrease α, the worst-case efficiency improves from 12.6% to 12.7% but average efficiency is reduced from 13.7% to 12.7%. This indicates that the trade-offs between the highest and the smallest efficiency are strong. It also stresses the point that it would be perhaps preferable to simply use the expected value design since the benefits in the lower tail in the efficiency are insignificant.

In terms of computational performance, all models were implemented in GAMS and solved with CONOPT. The problems in the first and second cases contained around 16,000 variables and were solved in around 4 min. In the third case the problems contained around 80,000 variables and were solved in 2–4 h. We would like to stress that we also tried global optimization solvers such as BARON to find global solutions but such solvers were not capable of dealing with the complexity of the physical model used. Therefore, our approach is to consider initialization strategies to try to

Table 6
CVaR designs for Case I: variability in $T^{HS}(\Xi)$ and at fixed $\eta_T(\Xi) = 90\%$.

	$T^{HS}(\Xi)$ in (°C)	130	135	140	145	150
$\alpha = 1/5$	$\eta(\Xi)$	16.5%	16.5%	16.5%	16.5%	16.5%
$z_{C_3H_3F_5} = 0.29$	$\mathbb{E}[\eta(\Xi)]$			16.5%		
$z_{C_4} = 0.004$	VaR			16.5%		
$z_{C_5} = 0.706$	CVaR			16.5%		
$\alpha = 2/5$	$\eta(\Xi)$	16.4%	16.7%	16.7%	16.7%	16.7%
$z_{C_3H_3F_5} = 0.081$	$\mathbb{E}[\eta(\Xi)]$			16.6%		
$z_{C_4} = 0.103$	VaR			16.7%		
$z_{C_5} = 0.816$	CVaR			16.6%		
$\alpha = 3/5$	$\eta(\Xi)$	16.4%	16.7%	16.7%	16.7%	16.7%
$z_{C_3H_3F_5} = 0.384$	$\mathbb{E}[\eta(\Xi)]$			16.6%		
$z_{C_4} = 0.072$	VaR			16.7%		
$z_{C_5} = 0.544$	CVaR			16.6%		
$\alpha = 4/5$	$\eta(\Xi)$	16.4%	16.7%	16.7%	16.7%	16.7%
$z_{C_3H_3F_5} = 0.384$	$\mathbb{E}[\eta(\Xi)]$			16.6%		
$z_{C_4} = 0.072$	VaR			16.7%		
$z_{C_5} = 0.544$	CVaR			16.6%		
$\alpha = 5/5$	$\eta(\Xi)$	16.0%	16.8%	16.8%	16.8%	16.8%
$z_{C_3H_3F_5} = 0.382$	$\mathbb{E}[\eta(\Xi)]$			16.6%		
$z_{C_4} = 0.059$	VaR			16.8%		
$z_{C_5} = 0.559$	CVaR			16.6%		

Table 7
Perfect information design for Case II: variability in $\eta_T(\Xi)$ and fixed $T^{HS}(\Xi) = 150$ (°C).

	$\eta_T(\Xi)$				
	90%	85%	80%	75%	70%
$z_{C_3H_3F_5}$	–	0.218	0.197	0.074	0.197
$z_{C_5F_{12}}$	–	–	–	–	–
z_{C_4}	0.35	–	–	0.106	–
z_{C_5}	0.65	0.782	0.803	0.820	0.803
$\eta(\Xi)$	18.2%	17.4%	16.3%	15.3%	14.2%
$\mathbb{E}[\eta(\Xi)]$			16.3%		

Table 8
Stochastic design for Case II: variability in $\eta_T(\Xi)$ and fixed $T^{HS}(\Xi) = 150$ (°C).

	$\eta_T(\Xi)$				
	90%	85%	80%	75%	70%
$z_{C_3H_3F_5}$			–		
$z_{C_5F_{12}}$			0.957		
z_{C_4}			0.043		
z_{C_5}			–		
$\eta(\Xi)$	14.5%	13.7%	12.8%	12.0%	11.2%
$\mathbb{E}[\eta(\Xi)]$			12.8%		

Table 9
CVaR designs for Case II: variability in $\eta_T(\Xi)$ and at fixed $T^{HS}(\Xi) = 150$ (°C). The optimal mixture composition is the same for any α value: 0.957 C_5F_{12} and 0.043 C_4.

	$\eta_T(\Xi)$	90%	85%	80%	75%	70%
$\alpha = 1/5$	$\eta(\Xi)$	14.5%	13.7%	12.8%	12.0%	11.2%
	$\mathbb{E}[\eta(\Xi)]$			12.8%		
	VaR			11.9%		
	CVaR			11.1%		
$\alpha = 2/5$	$\eta(\Xi)$	14.5%	13.7%	12.8%	12.0%	11.2%
	$\mathbb{E}[\eta(\Xi)]$			12.8%		
	VaR			12.8%		
	CVaR			11.6%		
$\alpha = 3/5$	$\eta(\Xi)$	14.5%	13.7%	12.8%	12.0%	11.2%
	$\mathbb{E}[\eta(\Xi)]$			12.8%		
	VaR			12.8%		
	CVaR			11.9%		
$\alpha = 4/5$	$\eta(\Xi)$	14.5%	13.7%	12.8%	12.0%	11.2%
	$\mathbb{E}[\eta(\Xi)]$			12.8%		
	VaR			13.7%		
	CVaR			12.4%		
$\alpha = 5/5$	$\eta(\Xi)$	14.5%	13.7%	12.8%	12.0%	11.2%
	$\mathbb{E}[\eta(\Xi)]$			12.8%		
	VaR			14.8%		
	CVaR			12.8%		

Table 10
Stochastic design for Case III: variability in $\eta_T(\Xi)$ and $T^{HS}(\Xi)$.

Optimal mixture composition					
$z_{C_3H_3F_5}$			–		
z_{C_4}			0.362		
z_{C_5}			0.638		
Overall cycle efficiency $\eta(\Xi)$					
			$\eta_T(\Xi)$		
$T^{HS}(\Xi)$	90%	85%	80%	75%	70%
130	16.3%	15.3%	14.4%	13.5%	12.5%
135	16.9%	16.0%	15.0%	14.0%	13.0%
140	17.5%	16.5%	15.5%	14.5%	13.5%
145	17.9%	16.9%	15.9%	14.8%	13.8%
150	18.2%	17.2%	16.2%	15.1%	14.1%
$\mathbb{E}[\eta(\Xi)]$			15.4%		

Table 11
CVaR design ($\alpha = 0.2$) for Case III: variability in $\eta_T(\Xi)$ and $T^{HS}(\Xi)$.

Optimal mixture composition					
$z_{C_3H_3F_5}$			0.028		
z_{C_4}			0.333		
z_{C_5}			0.639		
			Overall cycle efficiency $\eta(\Xi)$		
			$\eta_T(\Xi)$		
$T^{HS}(\Xi)$	90%	85%	80%	75%	70%
130	13.7%	13.7%	13.7%	13.6%	12.6%
135	13.7%	13.7%	13.7%	13.7%	13.1%
140	13.7%	13.7%	13.7%	13.7%	13.4%
145	13.7%	13.7%	13.7%	13.7%	13.7%
150	15.8%	15.0%	13.7%	13.7%	13.7%
$\mathbb{E}[\eta(\Xi)]$			13.7%		
VaR			13.3%		
CVaR			13.7%		

Table 12
CVaR design ($\alpha = 0.0$) for Case III: variability in $\eta_T(\Xi)$ and $T^{HS}(\Xi)$.

Optimal mixture composition					
$z_{C_3H_3F_5}$			–		
z_{C_4}			0.18		
z_{C_5}			0.82		
			Overall cycle efficiency $\eta(\Xi)$		
			$\eta_T(\Xi)$		
$T^{HS}(\Xi)$	90%	85%	80%	75%	70%
130	12.7%	12.7%	12.7%	12.7%	12.7%
135	12.7%	12.7%	12.7%	12.7%	12.7%
140	12.7%	12.7%	12.7%	12.7%	12.7%
145	12.7%	12.7%	12.7%	12.7%	12.7%
150	12.7%	12.7%	12.7%	12.7%	12.7%
$\mathbb{E}[\eta(\Xi)]$			12.7%		
VaR			12.7%		
CVaR			12.7%		

identify and bypass the presence of local optima. Based on the trends of our results with different scenarios under perfect information and stochastic designs for mean-variance and with CVaR for different probability levels α, we can conclude that our results are consistent and that high-quality solutions are being identified by the local solver CONOPT.

5. Conclusions

In this work, we address the problem of designing flexible multi-component organic fluids capable of withstanding variability in heat source temperatures and efficiencies of individual cycle equipment units. The design problem is cast as a nonlinear stochastic optimization problem and we incorporate risk metrics to handle extreme variability. We show that a stochastic optimization framework allows us to systematically trade-off performance of the working fluid under a variety of scenarios (e.g., inlet source temperatures and equipment efficiencies). With this, it is possible to design working fluids that remain robust in a wide range of operational conditions. We also find that significant flexibility of the working fluid can be obtained by using optimal concentrations as opposed to using single component mixtures. We also find that state-of-the-art nonlinear optimization solvers can handle highly complex stochastic optimization problems that incorporate detailed physical representations of the system.

Appendix A. Physical model and optimization formulation

In this section we present a detailed deterministic optimization formulation to simultaneously optimize the design of organic working fluids and of the ORC operating conditions.

A.1. Objective function

The objective is to maximize the efficiency of the cycle, which is denoted by η and given by:

$$\eta = \frac{W_{net}}{q_{IN}}. \tag{A.17}$$

The net work W_{net} and the heat inlet q_{IN} are computed based on the enthalpy changes at the subcooled and superheated points in the cycle:

$$\eta = \frac{(\widehat{H}_{over,high} - \widehat{H}_{over,low}) - (\hat{h}_{sub,high} - \hat{h}_{sub,low})}{(\widehat{H}_{over,high} - \hat{h}_{sub,high})} \tag{A.18}$$

where $\hat{h}_{sub,e}$ is the enthalpy of subcooled liquid and $\widehat{H}_{over,e}$ is the enthalpy of overheat vapor, also the subscript e is the pressure level (high and low). The efficiency equation takes into account the amount of heat absorbed and it is an indicator of the useful energy output to energy input ratio. Therefore, since W_{net} is related to the output power, the maximization of η and W_{net} is also an indirect

way of maximizing the output power. We highlight that other objective functions that account for detailed process economics are possible. Here, we use the efficiency because it is a metric that can be used in a general setting without having to quantify specific process economics.

A.2. Constraints

The constraints in the optimization model are given by thermodynamic relationships.

A.2.1. Enthalpy calculations

We first consider enthalpy calculations for the working fluid, enthalpy calculations for the heat source (heating) and, enthalpy calculations for cold source (cooling).

For the working fluid, the enthalpy of the saturated liquid mixture is calculated as [48]:

$$\hat{h}_e = h_0 + \sum_i^{N_C} z_i \left(\int_{T_0}^{T_{Be}} C_{pL,i}(T)dT + \int_{P_0}^{P_e} v_{L,Bei}(P)dP \right) + H_e^E, \quad \forall e \tag{A.19}$$

The subscript e is the pressure level (high and low), i is the subscript for mixture component, N_C is the number of components in the mixture, z_i is the composition of the mixture, and the subscript B denotes the bubble point. Symbol h_0 denotes the enthalpy at the reference state, $C_{pL,i}$ is the pure component liquid heat capacity (computed in (A.27)), H_e^E is the excess enthalpy for the liquid mixture and $v_{L,Bei}$ is the volume of saturated liquid (computed in (A.38)).

The enthalpy of the saturated vapor mixture is calculated as [48,49]:

$$\widehat{H}_e = \hat{h}_e - H_e^E + \sum_i^{N_C} z_i \left(\Delta h_{ie}^{LV} - H_{ie}^R + \int_{T_{Be}}^{T_{De}} C_{p,i}^{IG}(T)dT \right) + \widehat{H}_e^R, \quad \forall e \tag{A.20}$$

The subscript D is the dew point, Δh_{ie}^{LV} is the vaporization enthalpy change, $\widehat{H}_e^R$ is the residual enthalpy of vapor phase in the mixture, H_{ie}^R is the residual enthalpy of ideal gas and, $C_{p,i}^{IG}$ is the heat capacity of the ideal gas by Eq. (A.28).

The excess enthalpy of the liquid mixture is calculated by UNIFAC as [48,49]:

$$\frac{-H_e^E}{R_g T_{Be}^2} = \sum_i^{N_C} z_i (\log \gamma_{iBLe}), \quad \forall e \tag{A.21}$$

where $\log \gamma_{iBLe}$ is the natural logarithm of the activity coefficient at the bubble point and the subscript L is the liquid phase.

The residual enthalpy of the vapor phase mixture is calculated as [49–51]:

$$\frac{\widehat{H}_e^R}{R_g T_{De}} = (\hat{\alpha}_{De} -) \frac{\hat{a}'_e}{R_g \hat{b}} \log \frac{\widehat{Z}_{De}}{\widehat{Z}_{De} + \hat{\beta}_e} + \widehat{Z}_{De} - 1, \quad \forall e \tag{A.22}$$

where $\alpha_{De}, \beta_e, \widehat{Z}_{De}, a'_e$ and, $\hat{b}$ are variables of the Predictive Soave Redlich Kwong (PSRK) equation for mixtures (described later).

The residual enthalpy of ideal gas a component pure i is denoted as H_{ie}^R and calculated as [49–51]:

$$\frac{H_{ie}^R}{R_g T_{iBe}} = (\alpha_{iBe} -) \frac{a'_{ie}}{R_g b_i} \log \frac{Z_{ie}}{Z_{ie} + \beta_{iBe}} + Z_{ie} - 1, \quad \forall e \tag{A.23}$$

The vaporization enthalpy change is computed using Watson's equation [52]:

$$\Delta h_{ie}^{LV} = \Delta h_{b,i}^{LV} \left(\frac{1 - T_{r,iBe}}{1 - \frac{T_{b,i}}{T_{c,i}}} \right)^{0.375}, \quad \forall i, e \tag{A.24a}$$

where $\Delta h_{b,i}^{LV}$ is the change enthalpy at the normal boiling point.

$$\Delta h_{b,i}^{LV} = 1.093 R_g T_{c,i} T_{b,i} \left(\frac{ln P_{c,i} - 1.013}{0.93 - \frac{T_{b,i}}{T_{c,i}}} \right), \quad \forall i, e \tag{A.24b}$$

$T_{c,i}$ is the critical temperature, $T_{b,i}$ is the normal boiling temperature and, T_r is reduced temperature. The enthalpy of the heat source liquid is defined as [9]:

$$\Delta H_{HS,f} = \int_{T^{HS,OUT}}^{T_f^{HS}} C_{pL,HS}(T)dT, \quad \forall f \tag{A.25}$$

where the subscript f is de vaporization level $(B, 1, 2, \ldots, N_\Psi, D)$, T_f^{HS} is heat source temperature at vaporization level f, $T_{HS,OUT}$ is the outlet heat source temperature and, $C_{pL,HS}$ is the heat capacity of the heat source (computed in Eq. (A.27)).

The enthalpy change of the cold source is [9]:

$$\Delta H_{CS,f} = \int_{T^{CS,INT}}^{T_f^{CS}} C_{pL,CS}(T)dT, \quad \forall f \tag{A.26}$$

Likewise T_f^{CS} is cold source temperature at vaporization level, $T_{CS,INT}$ is the inlet temperature of cold source and, $C_{pL,CS}$ is the heat capacity of the cold source.

A.2.2. Heat capacity calculations

The liquid heat capacity is calculated as follows [53]:

$$C_{pL,i}(T) = C_{p,i}^{IG}(T) + 1.586 R_g + R_g \frac{0.49}{1 - \frac{T}{T_{c,i}}} + R_g \omega_i \left[4.2775 + \frac{6.3\left(1 - \frac{T}{T_{c,i}}\right)^{1/3}}{\frac{T}{T_{c,i}}} + \frac{0.4355}{1 - \frac{T}{T_{c,i}}} \right] \tag{A.27}$$

where ω_i is the acentric factor of component i. The ideal gas heat capacity is calculated as follows [53]:

$$C_{p,i}^{IG}(T) = C_{1,i} + C_{2,i} \left[\frac{\frac{C_{3,i}}{T}}{\sinh\left(\frac{C_{3,i}}{T}\right)} \right]^2 + C_{4,i} \left[\frac{\frac{C_{5,i}}{T}}{\cosh\left(\frac{C_{5,i}}{T}\right)} \right]^2 \tag{A.28}$$

$C_{1,i}, C_{2,i}, C_{3,i}, C_{4,i}$ are specific parameters of component i.

A.2.3. Energy balances

Energy balances in the two-phase region for the condenser are given by:

$$n_{HS} \Delta H_{HS,f} + \hat{h}_{sub,high} = \Psi_f (\widehat{H}_{high} - \hat{h}_{high}) + \hat{h}_{high}, \quad \forall f \tag{A.29a}$$

$$n_{HS} \Delta H_{HS,f} = q_{IN} \tag{A.29b}$$

$$q_{IN} = \widehat{H}_{over,high} - \hat{h}_{sub,high}. \tag{A.29c}$$

For the evaporator, they are given by:

$$n_{CS} \Delta H_{CS,f} + \hat{h}_{sub,low} = \Psi_f (\widehat{H}_{low} - \hat{h}_{low}) + \hat{h}_{sub,low}, \quad \forall f \tag{A.30a}$$

$$n_{CS} \Delta H_{CS,f} = q_{OUT} \tag{A.30b}$$

$$q_{OUT} = \widehat{H}_{over,low} - \hat{h}_{sub,low} \tag{A.30c}$$

Here, n_{HS} is the molar ratio between the heat source and the working fluid, n_{CS} is the molar ratio between the cold source and the working fluid, q_{IN} is the inlet heat and, q_{OUT} is the outlet heat. Otherwise $\widehat{H}_{high}$ is the enthalpy of vapor in the mixture and $\hat{h}_{high}$ enthalpy of liquid in the mixture, and Ψ_f is the vapor fraction that is 0 for

subscript $f = B$ and 1 for subscript $f = D$. Finally, $\Delta H_{HS,f}$ and $\Delta H_{CS,f}$ are changes enthalpy defined in Eqs. (A.25) and (A.26).

A.2.4. Entropy calculations

The entropy of the saturated liquid mixture is calculated as follows [48]:

$$\hat{s}_e = s_0 + \sum_i^{N_C} z_i \left(\int_{T_0}^{T_{Be}} \frac{C_{pL,i}}{T}(T)dT \right) + S_e^E, \quad \forall e \tag{A.31}$$

here S_e^E is the excess entropy and s_0 is the reference entropy. The entropy of the saturated vapor mixture is calculated as follows [48]:

$$\widehat{S}_e = \hat{s}_e - \widehat{S}_e^E + \sum_i^{N_C} z_i \left(\frac{\Delta h_{ie}^{LV}}{T_{Be}} - S_{ie}^R + \int_{T_{Be}}^{T_{De}} \frac{C_{p,i}^{IG}(T)}{T} dT \right) + \widehat{S}_e^R, \quad \forall e \tag{A.32}$$

here S_{ie}^R and $\widehat{S}_e^R$ are the residual entropies for pure components and the mixture, respectively. The excess entropy is calculated as follows [49–51]:

$$S_e^E = \frac{H_e^E - G_{BLe}^E}{T_{Be}}, \quad \forall e \tag{A.33}$$

where G_{BLe}^E is the Gibbs excess property. The residual entropy for component pure is calculated as [49–51]:

$$\frac{S_{ie}^R}{R_g} = \log(Z_{ie} - \beta_{iBe}) - \frac{a'_{ie}}{R_g b_i} \log \frac{Z_{ie}}{Z_{ie} + \beta_{iBe}}, \quad \forall i, e \tag{A.34}$$

The residual entropy for mixture is calculated as follows [49–51]:

$$\frac{\widehat{S}_e^R}{R_g} = \log(\widehat{Z}_e - \hat{\beta}_{Be}) - \frac{\hat{a}'_e}{R_g \hat{b}} \log \frac{\hat{Z}_e}{\hat{Z}_e + \hat{\beta}_{Be}}, \quad \forall e \tag{A.35}$$

A.2.5. Isentropic operation constraints

The isentropic operation constraints define the operating region for the pump and the turbine and are given by:

$$\hat{s}_{subS,high} = \hat{s}_{subS,low} \tag{A.36a}$$

$$\widehat{S}_{subS,high} = \widehat{S}_{subS,low} \tag{A.36b}$$

$$(\widehat{H}_{overS,high} - \widehat{H}_{overS,low}) = \eta_{ST}(\widehat{H}_{overS,high} - \widehat{H}_{overS,low}) \tag{A.36c}$$

$$(\hat{h}_{sub,high} - \hat{h}_{sub,low}) = \frac{1}{\eta_{SP}}(\hat{h}_{subS,high} - \hat{h}_{subS,low}) \tag{A.36d}$$

where *subS* is the subcool isentropic point and *overS* is the overheat isentropic point. Symbols η_{ST} and η_{SP} denote efficiency parameters for the turbine and pump respectively.

A.2.6. Compressed volume calculations

The correlation of Chang and Zhao (as a function of the pressure) is used to calculate the compressed volume [54]:

$$v_{L,ife}(P) = v_{L,ife}^{sat} \frac{A_{cz,ife} P_{c,i} + C_{cz}^{(D_{cz} - T_{r,ife})^{B_{cz,i}}} (P - P_{ife}^{sat})}{A_{cz,ife} P_{c,i} + C_{cz}(P - P_{ife}^{sat})} \tag{A.37a}$$

where C_{cz} and D_{cz} are constants, $v_{L,ife}^{sat}$ is the liquid volume at saturation temperature by Eq. (A.38), $P_{c,i}$ and $T_{r,ife}$ are the critical pressure and the reduced temperature, respectively. The coefficients $A_{cz,ife}$ and $B_{cz,i}$ are computed using the polynomials:

$$A_{cz,ife} = a_0 + a_1 T_{r,ife} + a_2 T_{r,ife}^3 + a_3 T_{r,ife}^6 + \frac{a_4}{T_{r,ife}} \tag{A.37b}$$

$$B_{cz,i} = b_{cz,0} + \omega_i b_{cz,1} \tag{A.37c}$$

where $a_0, a_1, a_2, a_3, a_4, b_{cz,0}, b_{cz,1}$ are given correlation constants [54].

A.2.7. Saturation liquid volume calculation

The saturated liquid volume is calculated using the Rackett equation [55].

$$v_{L,ife}^{sat} = v_{c,i} Z_{c,i}^{(1 - T_{r,ife})^{2/7}}, \quad \forall i, f, e \tag{A.38}$$

where $v_{c,i}$ and $Z_{c,i}$ are critical volumes and critical compressibility factor.

A.2.8. Vapor pressure calculations

The vapor pressure is calculated using the Riedel equation [56]

$$lnP_{ife}^{sat} = A_{R,i} - \frac{B_{R,i}}{T_{r,ife}} + C_{R,i} lnT_{r,ife} + D_{R,i} T_{r,ife}^6, \quad \forall i, f, e \tag{A.39a}$$

where its parameters are computed as:

$$A_{R,i} = -35 Q_{R,i} \tag{A.39b}$$

$$B_{R,i} = -36 Q_{R,i} \tag{A.39c}$$

$$C_{R,i} = 42 Q_{R,i} + \alpha_{Rc,i} \tag{A.39d}$$

$$D_{R,i} = -Q_{R,i} \tag{A.39e}$$

$$Q_{R,i} = 0.0838(3.758 - \alpha_{Rc,i}) \tag{A.39f}$$

$$\alpha_{Rc,i} = \frac{0.3149204 \Psi_{bR,i} + \log\left(\frac{P_{c,i}}{1.0135}\right)}{0.0838 \Psi_{bR,i} - \log \frac{T_{b,i}}{T_{c,i}}} \tag{A.39g}$$

$$\Psi_{bR,i} = -35 + 36 \frac{T_{c,i}}{T_{b,i}} + 42 \log \frac{T_{b,i}}{T_{c,i}} - \left(\frac{T_{b,i}}{T_{c,i}} \right)^6 \tag{A.39h}$$

A.2.9. Fugacity coefficient calculations

The fugacity coefficient is calculated using the PSRK (Predictive Soave-Redlich-Kwong) equation of state [50]. This is given by:

$$\log \hat{\phi}_{ife} = \frac{\beta_{ife}}{\hat{\beta}_{fe}} (\widehat{Z}_{fe} - \beta_{fe}) + \bar{\alpha}_{ife} \log \frac{\hat{Z_{fe}} + \hat{\beta_{fe}}}{\widehat{Z}_{fe}}, \quad \forall i, f, e \tag{A.40}$$

The dimensionless variables for pure species i is calculated by the standard SRK equation and variables PSRK for mixtures. The compressibility factor for pure specie and mixture are calculated as follow:

$$Z_{ie} = 1 + \beta_{iBe} - \alpha_{iBe} \beta_{iBe} \frac{1}{Z_{ie}} \frac{Z_{ie} - \beta_{iBe}}{(Z_{ie} + \beta_{iBe})}, \quad \forall i, e \tag{A.41a}$$

$$\widehat{Z}_{fe} = 1 + \hat{\beta}_{fe} - \hat{\alpha}_{fe} \hat{\beta}_{fe} \frac{1}{\widehat{Z}_{fe}} \frac{\widehat{Z}_{fe} - \hat{\beta}_{fe}}{(\widehat{Z}_{fe} + \hat{\beta}_{fe})}, \quad \forall f, e \tag{A.41b}$$

The molar partial variables are calculated as follows:

$$\bar{\alpha}_{ife} = \frac{1}{A_1} \left(\log \gamma_{ifVe} + \log \frac{\hat{\beta}_{fe}}{\beta_{ife}} + \frac{\beta_{ife}}{\hat{\beta}_{fe}} - 1 \right) + \alpha_{ife}, \quad \forall i, f, e \tag{A.42}$$

where γ_{ifVe} is the activity coefficient by Eq. (A.50). The rest of the dimensionless variables are computed from:

$$\alpha_{ife} = \frac{0.42748}{0.08664} \frac{1}{T_{r,ife}} [1 + c_{\omega,i}(1 - T_{r,ife}^{0.5})]^2, \quad \forall i, f, e \tag{A.43a}$$

$$\hat{\alpha}_{fe} = -\frac{1}{0.64663} \left(\frac{G_{fVe}^E}{R_g T_{fe}} + \sum_1^{N_C} x_{ifVe} \log \frac{\hat{\beta}_{fe}}{\beta_{ife}} \right) + \sum_i^{N_C} x_{ifVe} \alpha_{ife}, \quad \forall f, e \tag{A.43b}$$

$$\beta_{ife} = \frac{0.08664}{T_{r,ife}} \frac{P_e}{P_{c,i}}, \quad \forall i,f,e \tag{A.44a}$$

$$\hat{\beta}_{fe} = \sum_{i}^{N_C} x_{ifVe}\beta_{ife}, \quad \forall f,e \tag{A.44b}$$

where x_{ifVe} is mole fraction of vapor phase, and $c_{\omega,i}$ is a parameter of the acentric factor ω_i by Eq. (A.49). Moreover, the residual enthalpies are given by:

$$a'_{ie} = -0.42748 \frac{R_g^2 T_{c,i}}{P_{c,i}} [c_{w,i} + c_{w,i}^2 (1 - T_{r,iBe}^{0.5})] T_{r,iBe}^{-0.5}, \quad \forall i,e \tag{A.45a}$$

$$\hat{a}'_e = \hat{b}\left[\frac{1}{A_1}(G_e^E)'_T + \sum_{1}^{N_C} \frac{z_i}{b_i} a'_{ie} + \frac{R_g}{A_1}\sum_{i}^{N_C} z_i \log\frac{\hat{\beta}_{De}}{\beta_{iDe}}\right], \quad \forall e \tag{A.45b}$$

with coefficients:

$$b_i = 0.08664 \frac{R_g T_{c,i}}{P_{c,i}}, \quad \forall i \tag{A.46a}$$

$$\hat{b} = \sum_{i}^{N_C} z_i b_i, \quad \forall elabeleqbmix \tag{A.46b}$$

and where $(G_e^E)'_T$ is the Gibbs energy temperature derivative calculated from:

$$(G_e^E)'_T = R_g T_{De} \sum_{i}^{N_C} z_i (\log\gamma_{iDVe})'_T + \frac{G^E_{DVe}}{T_{De}}, \quad \forall e \tag{A.47}$$

The Gibbs excess property is calculated as:

$$\frac{G^E_{fpe}}{R_g T_{fe}} = \sum_{i}^{N_C} x_{ifpe} \log\gamma_{ifpe}, \quad \forall f,p,e \tag{A.48}$$

The accentric parameter is given by:

$$c_{\omega,i} = (0.48 + 1.574\omega_i - 0.176\omega_i^2). \tag{A.49}$$

A.2.10. Activity coefficient calculations

The activity coefficient is calculated using the UNIFAC method. The method combines the solution-of-functional-groups with a model for activity coefficients (UNIQUAC Functional-group Activity Coefficients), also using group-interaction parameters [57]. The activity coefficient is calculated as follows:

$$\log\gamma_{ifpe} = \log\gamma^C_{ifpe} + \log\gamma^R_{ifpe}, \quad \forall i,f,p,e \tag{A.50}$$

where γ^C_{ifpe} and $\log\gamma^R_{ifpe}$ are combinatorial coefficient and residual coefficient respectively, both of them dimensionless. The combinatorial coefficient (γ^C_{ifpe}) is given by:

$$\log\gamma^C_{ifpe} = \log\frac{r_i}{\sum_j^{N_C} r_j x_{ifpe}} + \frac{10}{2} q_i \log\frac{q_i \sum_j^{N_C} r_j x_{ifpe}}{r_i \sum_j^{N_C} q_j x_{ifpe}} + l_i - \frac{r_i}{\sum_j^{N_C} r_j x_{ifpe}} \sum_{j}^{N_C} x_{ifpe} l_j, \quad \forall i,f,p,e \tag{A.51a}$$

The subscripts i and j refers to mixture components. Moreover, r_i, r_j, q_i, l_i, l_j are dimensionless UNIFAC parameters and are given by:

$$r_i = \sum_{k}^{N_G} v_k^{(i)} R_k, \quad \forall i \tag{A.51b}$$

$$q_i = \sum_{k}^{N_G} v_k^{(i)} Q_k, \quad \forall i \tag{A.51c}$$

$$l_i = \frac{10}{2}(r_i - q_i) - (r_i - 1), \quad \forall i \tag{A.51d}$$

The residual coefficient (γ^R_{ifpe}) is given by:

$$\log\gamma^R_{ifpe} = \sum_{k}^{N_G} v_k^{(i)} (\log\Gamma_{kfpe} - \log\Gamma^{(i)}_{kfe}), \quad \forall i,f,p,e \tag{A.52a}$$

$$\log\Gamma^{(i)}_{kfe} = Q_k\left[1 - \log\left(\sum_m^{N_G}\theta_m^{(i)}\Psi_{mkfe}\right) - \sum_m^{N_G}\frac{\theta_m^{(i)}\Psi_{kmfe}}{\sum_n^{N_G}\theta_n^{(i)}\Psi_{nmfe}}\right], \quad \forall i,k,f,e \tag{A.52b}$$

$$\log\Gamma^{(i)}_{kfpe} = Q_k\left[1 - \log\left(\sum_m^{N_G}\theta_{mfpe}\Psi_{mkfe}\right) - \sum_m^{N_G}\frac{\theta_{mfpe}\Psi_{kmfe}}{\sum_n^{N_G}\theta_{nfpe}\Psi_{nmfe}}\right], \quad \forall i,k,f,e \tag{A.52c}$$

$$\theta_m^{(i)} = \frac{Q_m X_m^{(i)}}{\sum_n^{N_G} Q_n X_n^{(i)}}, \quad \forall i,m \tag{A.52d}$$

$$\theta_{mfpe} = \frac{Q_m X_{mfpe}}{\sum_n^{N_G} Q_n X_{nfpe}}, \quad \forall m,f,p,e \tag{A.52e}$$

$$X_m^{(i)} = \frac{v_m^{(i)}}{\sum_n^{N_G} v_n^{(i)}}, \quad \forall i,m \tag{A.52f}$$

$$X_{mfpe} = \frac{\sum_i^{N_C} x_{ifpe} v_m^{(i)}}{\sum_n^{N_C}(x_{ifpe}\sum_n^{N_G} v_n^{(i)})}, \quad \forall m,f,p,e \tag{A.52g}$$

$$\Psi_{mnfe} = exp\left(-\frac{a_{mn}}{T_{fe}}\right), \quad \forall m,n,f,p,e \tag{A.52h}$$

where Q_k, Q_m, Q_n, R_k are dimensionless UNIFAC parameters

A.2.11. Equilibrium calculations

The vapor-liquid equilibrium conditions are calculated using the Rachford-Rice equation [58]:

$$\sum_{i}^{N_C} \frac{z_i(1 - K_{ife})}{1 + \Psi_f(K_{ife} - 1)} = 0, \quad \forall f,e \tag{A.53}$$

where K_{ife} is the phase equilibrium ratio and is calculated from [49]:

$$K_{ife} = \frac{\gamma_{ifLe} P^{sat}_{ife} \phi^{sat}_{ife} exp\int_{P^{sat}_{ife}}^{P_e} \frac{v_{Life}(P)}{R_g T_{fe}} dP}{\hat{\phi}_{ife} P_e}, \quad \forall i,f,e \tag{A.54}$$

A.2.12. Mole fraction and compositions

The mol fraction and composition of the phases satisfy:

$$\sum_{i}^{N_C} z_i = 1 \tag{A.55a}$$

$$\sum_{i}^{N_C} x_{ifpe} = 1 \tag{A.55b}$$

where the subscript p denotes the phase (liquid/vapor). The compositions of the phases at equilibrium are calculated as [49]:

$$x_{ifLe} = \frac{z_i}{1 + \Psi_f(K_{ife} - 1)}, \quad \forall i,f,e \tag{A.56a}$$

$$x_{ifVe} = \frac{z_i K_{ife}}{1 + \Psi_f(K_{ife} - 1)}, \quad \forall i,f,e \tag{A.56b}$$

A.2.13. Temperature constraints

Temperature constraints are imposed to achieve heat exchange between the working fluid and heat source. In the two-phase region, the constraints are given by [9]:

$$T_{f,high} + \Delta T^{S}_{min} \leqslant T^{HS}_{f}, \quad \forall f \tag{A.57a}$$

$$T_{f,low} - \Delta T^{S}_{min} \geqslant T^{CS}_{f}, \quad \forall f \tag{A.57b}$$

In the single-phase regions, the temperature constraints are:

$$\widehat{T}_{sub,high} + \Delta T^{S}_{min} \leqslant T^{HS,OUT} \tag{A.58a}$$

$$\widehat{T}_{over,high} + \Delta T^{S}_{min} \leqslant T^{HS,IN} \tag{A.58b}$$

$$\widehat{T}_{sub,low} - \Delta T^{S}_{min} \geqslant T^{CS,IN} \tag{A.58c}$$

$$\widehat{T}_{over,low} - \Delta T^{S}_{min} \geqslant T^{CS,OUT} \tag{A.58d}$$

A.2.14. Pressure constraints

The cycle pressure constraints are given by:

$$P_{high} \geqslant P_{low} + \Delta P_{min} \tag{A.59}$$

and where ΔP_{min} is the minimum pressure change of the cycle.

Appendix B. Nomenclature

B.1. subscripts

$d = sub, subS, over, overS$	Subcool, subcool isentropic, overheat, overheat isentropic points
$e = low, high$	Pressure level
$f = B, 1, 2, 3, D$	Vaporization level
$i, j = 1, 2, \ldots, N_C$	Mixture components
$k, m, n = 1, 2, \ldots, N_G$	UNIFAC functional group
$p = L, V$	Liquid and vapor phase

B.2. Variables

a'_{ie}	Pure temperature derivative [cm^6 bar mol^{-2} K^{-1}]
$\hat{a}'_{e}$	Mixture temperature derivative [cm^6 bar mol^{-2} K^{-1}]
$A_{cz,ife}$	Chanz Zhao polynomial [Dimensionless]
$\hat{b}$	Mixture EOS variable [cm^3 mol^{-1}]
G^{E}_{fpe}	Gibbs excess function [kJ kmol^{-1}]
$(G^{E}_{e})'_{T}$	Gibbs excess temperature derivative [kJ kmol^{-1}]
H^{E}_{e}	Excess enthalpy [kJ kmol^{-1}]
H^{R}_{ie}	Pure residual enthalpy [kJ kmol^{-1}]
$\widehat{H}_{d,e}$	Overheat vapor enthalpy [kJ kmol^{-1}]
$\hat{h}_{d,e}$	Subcool liquid enthalpy [kJ kmol^{-1}]
$\widehat{H}^{R}_{e}$	Mixture residual enthalpy [kJ kmol^{-1}]
h_0	Reference enthalpy [kJ kmol^{-1}]
K_{ife}	Equilibrium ratio [Dimensionless]
n_{HS}	Heat source fluid mole to working fluid ratio [Dimensionless]
n_{CS}	Cold source fluid mole to working fluid ratio [Dimensionless]
$P_{c,i}$	Critical pressure [bar]
P_e	Pressure [bar]
P^{sat}_{ife}	Saturation pressure [bar]
P_0	Reference pressure [bar]
q_{IN}	Input heat [kJ kmol^{-1}]
q_{OUT}	Output heat [kJ kmol^{-1}]
R_g	Ideal gas constant [kJ kmol^{-1} K^{-1}]
S^{E}_{e}	Excess entropy [kJ kmol^{-1} K^{-1}]
S^{R}_{ie}	Pure residual entropy [kJ kmol^{-1} K^{-1}]
$\hat{s}_e$	Mixture saturated vapor entropy [kJ kmol^{-1} K^{-1}]
$\hat{s}_{d,e}$	Subcool liquid entropy [kJ kmol^{-1} K^{-1}]
$\widehat{S}_{d,e}$	Overheat vapor entropy [kJ kmol^{-1} K^{-1}]
$\widehat{S}^{R}_{e}$	Mixture residual entropy [kJ kmol^{-1} K^{-1}]
s_0	Reference entropy [kJ kmol^{-1} K^{-1}]
$T_{b,i}$	Normal boiling temperature [K]
$T_{c,i}$	Critical temperature [K]
$T^{CS,IN}$	Cold fluid inlet temperature [K]
$T^{CS,OUT}$	Cold fluid outlet temperature [K]
T_{fe}	Working fluid temperature [K]
T^{CS}_{f}	Heat source fluid temperature [K]
T^{HS}_{f}	Heat sink fluid temperature [K]
$T^{HS,OUT}$	Hot fluid outlet temperature [K]
$T^{HS,IN}$	Hot fluid inlet temperature [K]
$T_{r,ife}$	Reduced temperature [K]
T_0	Reference temperature [K]
W_{net}	Net work [kJ kmol^{-1}]
x_{ifpe}	Mole fraction [Dimensionless]
$X^{(i)}_{m}$	Group mole fraction for pure i [Dimensionless]
X_{mfpe}	Group mole fraction [Dimensionless]
$X^{(i)}_{n}$	Group mole fraction for pure j [Dimensionless]
X_{nfpe}	Group mole fraction [Dimensionless]
z_i	Global composition [Dimensionless]
$Z_{c,i}$	Critical compressibility factor [Dimensionless]
Z_{ie}	Pure compressibility factor [Dimensionless]
$\widehat{Z}_{fe}$	Mixture compressibility factor [Dimensionless]
α_{ife}	EOS variable [Dimensionless]
$\bar{\alpha}_{ife}$	Molar partial [Dimensionless]
$\hat{\alpha}_{fe}$	EOS mixture variable [Dimensionless]
β_{ife}	Pure EOS variable [Dimensionless]
$\hat{\beta}_{fe}$	Mixture EOS variable [Dimensionless]
$\Delta h^{LV}_{b,i}$	Normal boiling point pure vaporization enthalpy [kJ kmol^{-1}]
Δh^{LV}_{ie}	Pure vaporization enthalpy change [kJ kmol^{-1}]
$\Delta H_{HS,f}$	Heat source enthalpy change [kJ kmol^{-1}]
$\Delta H_{CS,f}$	Heat sink enthalpy change [kJ kmol^{-1}]
ΔT^{S}_{min}	Profile minimum temperature difference [K]
ΔP_{min}	Minimum pressure change of the cycle [bar]
η	Global efficiency [Dimensionless]
η_{ST}	Turbine isentropic efficiency [Dimensionless]
η_{SP}	Pump isentropic efficiency [Dimensionless]
ϕ^{sat}_{ife}	Pure saturation fugacity coefficient [Dimensionless]
$\hat{\phi}_{ife}$	Mixture fugacity coefficient [Dimensionless]
γ_{ifpe}	Activity coefficient [Dimensionless]
$(\gamma_{ifpe})'_{T}$	Activity coefficient temperature derivative K^{-1}
γ^{C}_{ifpe}	Combinatorial activity coefficient [Dimensionless]
γ^{R}_{ifpe}	Residual activity coefficient [Dimensionless]
Γ_{kfpe}	Residual activity contribution mixture of groups [Dimensionless]

(*continued on next page*)

$\Gamma_{kfe}^{(i)}$	Residual activity contribution for groups of pure i [Dimensionless]
$v_{L.ife}^{sat}$	Saturation liquid volume [$cm^3\ mol^{-1}$]
$v_{c,i}$	Critical volume [$cm^3\ mol^{-1}$]
$v_k^{(i)}$	UNIFAC group m frequency on molecule i [Dimensionless]
$v_m^{(i)}$	UNIFAC group m frequency on molecule i [Dimensionless]
$v_n^{(i)}$	UNIFAC group m frequency on molecule i [Dimensionless]
ω_i	Acentric factor [Dimensionless]
Ψ_{kmfe}	UNIFAC binary interaction variable [Dimensionless]
Ψ_{nmfe}	UNIFAC binary interaction variable [Dimensionless]
Ψ_f	Vaporization fraction [Dimensionless]
$\theta_m^{(i)}$	UNIFAC area fraction variable for pure i [Dimensionless]
$\theta_n^{(i)}$	UNIFAC area fraction variable for pure i [Dimensionless]
θ_{mfpe}	UNIFAC area fraction variable [Dimensionless]
θ_{nfpe}	UNIFAC area fraction variable [Dimensionless]

B.3. Other symbols

x	Design variable
y	Operational variable
ξ	Realization of random variable
Ξ	Random variable
p_ξ	Probabilities
Ω	Scenario set
$\varphi(\cdot)$	Statistical function
$f(\cdot)$	Objective function
$\mathbb{E}$	Expected value
$\mathbb{V}$	Variance
κ	Weight
t	Auxiliary variable
α	Probability level
$\mathbb{D}_\kappa$	Dispersion metric
VaR	Value at risk
CVaR	Conditional value at risk

References

[1] Quolin S, Van Den Broek M, Declaye S, Dewallef P, Lemort V. Techno-economic survey of organic Rankine cycle (ORC) systems. Renew Sustain Energy Rev 2013;22:168–86.

[2] Hung TC, Shai TY, Wang SK. A review of organic Rankine cycles (ORCs) for the recovery of low-grade waste heat. Energy 1997;22:661–7.

[3] Wang ZQ, Zhou NJ, Guo J, Wang XY. Fluid selection and parametric optimization of organic Rankine cycle using low temperature waste heat. Energy 2012;40:107–15.

[4] Ayu TT, Hailu MH, Atnaw SM. Energy audit and waste heat recovery system design for a cement rotary kiln in Ethiopia: a case study. Int J Automot Mech Eng 2015;12:2983–3002.

[5] Yamamoto T, Furuhata T, Arai N, Mori K. Design and testing of the organic Rankine cycle. Energy 2001;26:239–51.

[6] Galanis N, Cayer E, Roy P, Denis ES, Desilets M. Electricity generation from low temperature sources. J Appl Fluid Mech 2009;2:55–67.

[7] Saleh B, Koglbauer G, Wendland M, Fischer J. Working fluids for low-temperature organic Rankine cycles. Energy 2007;32:1210–21.

[8] PLajorla J. Electricity from industrial waste heat using high-speed organic Rankine cycle (ORC). Int J Prod Econ 1995;41:227–35.

[9] Molina-Thierry DP, Flores-Tlacuahuac A. Simultaneous optimal design of organic mixtures and Rankine cycles for low-temperature energy recovery. Ind Eng Chem Res 2015;54:3367–83.

[10] Papadopoulos AI, Stijepovic M, Linke P. On the systematic design and selection of optimal working fluids for organic Rankine cycles. Appl Therm Eng 2010;30:760–9.

[11] Heberle Florian, Brüggemann Dieter. Thermo-economic analysis of zeotropic mixtures and pure working fluids in organic Rankine cycles for waste heat recovery. Energies 2016;9(4):226.

[12] Oyewunmi Oyeniyi A, Taleb Aly I, Haslam Andrew J, Markides Christos N. On the use of SAFT-VR Mie for assessing large-glide fluorocarbon working-fluid mixtures in organic Rankine cycles. Appl Energy 2016;163:263–82.

[13] Song Jian, Gu Chun-wei. Analysis of ORC (organic Rankine cycle) systems with pure hydrocarbons and mixtures of hydrocarbon and retardant for engine waste heat recovery. Appl Therm Eng 2015;89:693–702.

[14] Benato Alberto, Macor Alarico. Biogas engine waste heat recovery using organic Rankine cycle. Energies 2017;10(3):327.

[15] Heberle Florian, Brüggemann Dieter. Thermo-economic evaluation of organic Rankine cycles for geothermal power generation using zeotropic mixtures. Energies 2015;8(3):2097–124.

[16] Bao J, Zhao L. A review of working fluid and expander selections for organic Rankine cycle. Renew Sustain Energy Rev 2013;24:325–42.

[17] Chys M, Van den Broek M, Vanslambrouck B, De Paepeb M. Potential of zeotropic mixtures as working fluids in organic Rankine cycles. Energy 2012;44:623–32.

[18] Papadopoulos AI, Stijepovic MZ, Linke Patrick, Seferlis P, Voutetakis S. Toward optimum working fluid mixtures for organic Rankine cycles using molecular design and sensitivity analysis. Ind Eng Chem Res 2013;52:12116–33.

[19] Yin H, Sabau SA, Conklin CJ, McFarlane J, Qualls AL. Mixtures of SF_6-CO_2 as working fluids for geothermal power plants. Appl Energy 2013;106:243–53.

[20] Shu G, Gao Y, Tian H, Wei H, Liang X. Study of mixtures based on hydrocarbons used in ORC (organic Rankine cycle) for engine waste heat recovery. Energy 2014;74:428–38.

[21] Andreasen JG, Larsen U, Knudsen T, Pierobon L, Haglind F. Selection and optimization of pure and mixed working fluids for low grade heat utilization using organic Rankine cycles. Energy 2014;73:204–13.

[22] Yang K, Zhang H, Wang Z, Zhang J, Yang F, Wang E. Study of zeotropic mixtures of ORC (organic Rankine cycle) under engine various operating conditions. Energy 2013;58:494–510.

[23] Wang JL, Zhao L, Wang XD. A comparative study of pure and zeotropic mixtures in low-temperature solar Rankine cycle. Appl Energy 2010;87:3366–73.

[24] Zhao Li, Bao J. Thermodynamic analysis of organic Rankine cycle using zeotropic mixtures. Appl Energy 2014;130:748–56.

[25] Long Le V, Kheiri A, Feidt M, Pelloux-Prayer S. Thermodynamic and economic optimizations of a waste heat to power plant driven by a subcritical ORC (organic Rankine cycle) using pure or zeotropic working fluid. Energy 2014;78:622–38.

[26] You-Rong L, Mei-Tang D, Chun-Mei W, Shuang-Ying W, Liu Ch. Potential of organic Rankine cycle using zeotropic mixtures as working fluids for waste heat recovery. Energy 2014;77:509–19.

[27] Collings P, Yu Z, Wang E. A dynamic organic Rankine cycle using a zeotropic mixture as the working fluid with composition tuning to match changing ambient conditions. Appl Energy 2016;171:581–91.

[28] Sadeghi M, Nemati A, Ghavimi A, Yari M. Thermodynamic analysis and multi-objective optimization of various ORC (organic Rankine cycle) configurations using zeotropic mixtures. Energy 2016;109:791–802.

[29] Oyewunmi Oyeniyi A, Markides Christos N. Thermo-economic and heat transfer optimization of working-fluid mixtures in a low-temperature organic Rankine cycle system. Energies 2016;9(6):448.

[30] Liu Q, Shen A, Duan Y. Parametric optimization and performance analyses of geothermal organic Rankine cycles using R600a/R601a mixtures as working fluids. Appl Energy 2015;148:410–20.

[31] Feng Y, Hung T, Zhang Y, Li B, Yang J, Shi Y. Performance comparison of low-grade ORCs (organic Rankine cycles) using R245fa, pentane and their mixtures based on the thermoeconomic multi-objective optimization and decision makings. Appl Energy 2015;93:2018–29.

[32] Feng Y, Zhang Y, Li B, Yang J, Shi Y. Sensitivity analysis and thermoeconomic comparison of ORCs (organic Rankine cycles) for low temperature waste heat recovery. Energy 2015;82:664–77.

[33] Habka M, Ajib S. Evaluation of mixtures performances in organic Rankine cycle when utilizing the geothermal water with and without cogeneration. Appl Energy 2015;154:567–76.

[34] Papadopoulos AI, Stijepovic MZ, Linke Patrick, Seferlis P. Molecular design of working fluid mixtures for organic Rankine cycles. Comput Aided Process Eng 2013;32:289–94.

[35] Linke Patrick, Papadopoulos AI, Seferlis Panos. Systematic methods for working fluid selection and the design, integration and control of organic Rankine cycles – a review. Energies 2015;8:4755–801.

[36] Frutiger J, Andreasen J, Liu W, Spliethoff H, Haglind F, Abildskov J, et al. Working fluid selection for organic Rankine cycles e impact of uncertainty of fluid properties. Energy 2016;109:987–97.

[37] Schwöbel Johannes AH, Preißinger Markus, Brüggemann Dieter, Klamt Andreas. High-throughput-screening of working fluids for the organic Rankine cycle (ORC) based on COSMO-RS and thermodynamic process simulations. Ind Eng Chem Res 2016.

[38] Chen H, Goswami D, Stefanakos E. A review of thermodynamic cycles and working fluids for the conversion of low-grade heat. Renew Sustain Energy Rev 2010;14:3059–67.

[39] Sung T, Yun E, Kima H, Yoon S, Choi B, Kima K, et al. Performance characteristics of a 200-kW organic Rankine cycle system in a steel processing plant. Appl Energy 2016;183:623–35.
[40] Di Battista D, Cipollone R, Villante C, Fornari C, Mauriello M. The potential of mixtures of pure fluids in ORC-based power units fed by exhaust gases in internal combustion engines. Energy Proc 2016;101:1264–71.
[41] Stijepovic MZ, Linke Patrick, Papadopoulos AI, Grujic AS. On the role of working fluid properties in organic Rankine cycle performance. Energies 2012;36:406–13.
[42] Kalina AI. Method and apparatus for converting low temperature heat to electric power. <http://www.google.co.in/patents/US5029444>; 07 1991.
[43] Angelino G, Di Paliano P Colonna. Multicomponent working fluids for organic Rankine cycles (ORCs). Energy 1998;23:449–63.
[44] Rockafellar TR, Uryasev S, Zabarankin M. Deviation measures in risk analysis and optimization. In: Research report; 2002. p. 1–27.
[45] Rockafellar TR, Uryasev S, Zabarankin M. Generalized deviations in risk analysis. Financ Stoch 2006;10:51–74.
[46] Birge JR, Louveaux F. Introduction to stochastic programming; 2011. ISBN 978-1-4614-0236-7.
[47] Uryasev Stanislav. Conditional value at risk: optimization algorithms and applications. In: Financial engineering news. University of Florida; 2000. p. 1–6.
[48] Smith J, Van Ness HC, Abbott MM. Introduction to chemical engineering thermodynamics; 2005. ISBN 978-970-10-6147-3.
[49] Poling BE, Prausnitz JM, O'Connell JP. The properties of gases and liquids; 2001. ISBN 0-07-011682-2.
[50] Holderbaum T, Gmehling J. PSRK: a group contribution equation of state based on UNIFAC. Fluid Phase Equilib 1991;70:251–65.
[51] Fischer K, Gmehling J. Further development, status and results of the PSRK method for the prediction of vapor-liquid equilibria and gas solubilities. Fluid Phase Equilib 1996;121:185–206.
[52] Watson KM. Prediction of critical temperatures and heats of vaporization. Ind Eng Chem 1931;23:360–4.
[53] Aly Fouad A, Lee LLoyd L. Self-consistent equations for calculating the ideal gas heat capacity, enthalpy, and entropy. Fluid Phase Equilib 1981;6:169–79.
[54] Chang C, Zhao X. A new generalized equation for predicting volumes of compressed liquids. Fluid Phase Equilib 1989;58:231–8.
[55] Yamada T, Gunn RD. Satured liquid molar volumes. The Rackett equation. J Chem Eng Data 1973;18:234–6.
[56] Riedel L. Extension of the theorem of corresponding states III. Critical coefficient, density of saturated vapor, and latent heat of vaporization. Chem Ing Tech 1954;26:679–83.
[57] Fredenslund A, Jones LR, Prausnitz JM. Group-contribution estimation of activity coefficients in nonideal liquid mixtures. AIChE J 1975;21:1086–99.
[58] Seader JD, Henley JE, Keith RD. Separation process principles: chemical and biochemical operations; 2011. ISBN 978-0-470-48183-7.